Showcasing research from Professor Dawid Janas' Functional Nanomaterials Group at Silesian University of Technology, Poland.

Programing optical properties of single-walled carbon nanotubes with benzoyl peroxide derivatives of tailored chemical characteristics

The application of custom-made benzoyl peroxide analogs opens new avenues for tuning the optical properties of single-walled carbon nanotubes. Covalent surface modification of SWCNTs with these reactants significantly enhances radiative recombination of excitons, boosting the potential of these nanomaterials for cutting-edge photonics applications.

Image reproduced by permission of Dawid Janas from *Mater. Horiz.*, 2025, **12**, 9040.

As featured in:

See Andrzej Dzienia, Dawid Janas *et al.*, *Mater. Horiz.*, 2025, **12**, 9040.

ROYAL SOCIETY OF CHEMISTRY

rsc.li/materials-horizons

Registered charity number: 207890

Materials Horizons

ROYAL SOCIETY OF CHEMISTRY

COMMUNICATION

View Article Online
View Journal | View Issue

Cite this: *Mater. Horiz.*, 2025, **12**, 9040

Received 13th June 2025,
Accepted 24th September 2025

DOI: 10.1039/d5mh01129a

rsc.li/materials-horizons

Programing optical properties of single-walled carbon nanotubes with benzoyl peroxide derivatives of tailored chemical characteristics

Andrzej Dzienia,* Patrycja Taborowska, Paweł Kubica-Cypek and Dawid Janas*

Semiconducting single-walled carbon nanotubes (SWCNTs) have great potential for optoelectronics and photonics, further enhanced by covalent functionalization. However, scalable and controlled surface modification is challenging due to complex methodologies and unstable reagents. Benzoyl peroxide (BPO) has emerged as a simple alternative for introducing luminescent defects into SWCNTs. Yet, the lack of understanding of its radical chemistry limits precise defect engineering using BPOs. This is a major obstacle to the effective application of BPO in chemistry, despite its widespread use as a radical initiator. We present a thorough investigation into the radical chemistry of self-synthesized BPOs for functionalizing polymer-wrapped (6,5) and (7,5) SWCNTs in non-polar solvents, providing critical insights into the decomposition of BPO and its analogs. By varying the electronic and steric properties of typically unavailable BPO derivatives, we demonstrate tunability over the photoluminescence characteristics of SWCNTs, allowing control over defect density and light emission wavelength. This toolbox of BPO derivatives, created with simple radical chemistry and accessible organic precursors, alongside clarified structure–property relationships, facilitates effective implementation of BPO in chemical transformations and meticulous engineering of luminescent defects in SWCNTs for optoelectronic applications. Notably, this research offers insights into why SWCNTs modified with electron-deficient reactants provide the best optical characteristics.

New concepts

With their structure-controlled fluorescence, semiconducting single-walled carbon nanotubes (SWCNTs) hold significant promise for photonics. Moreover, a slight chemical modification of the material can further enhance its optical characteristics. However, despite substantial progress in this area of research, the nature of the underlying chemical transformations remains unclear. Radical reactions are inherently complex, making it challenging to fully understand the phenomena at the nanoscale. To approach this long-awaited goal more closely, we thoroughly studied the decomposition of a wide range of self-synthesized, commercially unavailable benzoyl peroxide (BPO) derivatives and their potential for SWCNT functionalization. Despite the common use of BPO as a radical initiator in chemistry, its mechanism of action is ambiguous. Nonetheless, the results of this study provide significant insight into the mechanics of its decay, emphasizing the interdisciplinary importance of this work. From the perspective of low-dimensional materials for photonics, the outcomes of this synthetically demanding project demonstrate how the optical properties of SWCNTs may be tailored in a straightforward way. Finally, the article explains how attaching electron-deficient functional groups to SWCNTs modifies the photophysics of the material, enabling more precise exciton engineering.

1. Introduction

Semiconducting single-walled carbon nanotubes (s-SWCNTs) hold considerable promise for applications in optoelectronics, photonics, telecommunications, and quantum information technologies.[1–3] One of the key merits of SWCNTs is that their characteristics, including optical properties, are determined by their structure. Consequently, their optical absorption and emission wavelengths can be adjusted for a specific application. Taking into account that their capacity for structure-dependent light emission spans from the visible to the near-infrared range (NIR), SWCNTs are very valuable materials for basic and applied research. Unfortunately, a critical challenge in utilizing SWCNTs in optoelectronics and photonics is their relatively low photoluminescence quantum yield (PLQY), which greatly diminishes their implementation potential. Pristine SWCNTs typically exhibit poor PLQY (on the order of 0.5–2%[4,5]), meaning that the light they emit is unsatisfactorily dim.

Chemical functionalization of SWCNTs in water[6–8] or organic solvents[9–11] has emerged as a promising approach to overcome this limitation. Firstly, the inclusion of luminescent defects in SWCNTs, often referred to as Organic Color Centers (OCCs) or quantum defects,[12] modifies the electronic structure

Department of Chemistry, Silesian University of Technology, B. Krzywoustego 4, 44-100, Gliwice, Poland. E-mail: Andrzej.Dzienia@polsl.pl, Dawid.Janas@polsl.pl

of SWCNTs, traps the mobile excitons, and makes the radiative recombination of excitons more likely. Secondly, the formation of these exciton traps generates new emission peaks, such as E_{11}^{*} and E_{11}^{*-}, which are redshifted relative to the native optical transition of SWCNTs (E_{11}). The extent of this shift, as well as the intensity of the newly formed peaks, depends on the nature of the attached functional groups[12] and their overall number on the SWCNT surface. For example, the E_{11}^{*} peak is typically redshifted by 120–160 nm compared to E_{11},[13] while further redshifted peaks, such as E_{11}^{*-}, can be induced by the attachment of divalent functional groups or through high degrees of functionalization.[5,14] Consequently, the PLQY of SWCNTs can be increased, thereby reaching 4%[5] or more. In light of the foregoing, it is evident that the development of effective functionalization strategies to improve the optical properties of SWCNTs is essential.

Diverse chemical modification methods enable the implantation of defects in SWCNTs, employing principles from both inorganic and organic chemistry, depending on the type of functional group introduced and the reagents utilized. The inorganic approach primarily focuses on oxidation, using reactive oxygen species. Effective oxidation methods include the use of hydrogen peroxide (H_2O_2), ozone (O_3), sodium hypochlorite (NaClO), unsaturated fatty acids, and organosulfur compounds.[8] The more complex organic strategy adapts a range of reactions typical of organic chemistry. Key strategies encompass diazonium coupling, employing diazonium salts ($[ArN_2]X$),[15] variants of reductive alkylation, such as Billups–Birch reduction (using lithium in liquid ammonia, Li/NH_3, followed by alkylation with RX) and alkylation using sodium naphthalenide (Na/naphthalene, then RBr). Alkylation methodologies also include dialkylation (*e.g.*, using RLi followed by RX).[16] Although these principal functionalization pathways – oxidation, alkylation, and arylation – provide the foundation for generating luminescent defects in SWCNTs that modulate their photoluminescence properties, they often lack the selectivity required for controlled defect implantation, limiting the potential for punctilious optical engineering of these nanomaterials.

To capitalize on the remarkable utility of benzoyl peroxide (BPO) in organic chemistry, we have recently explored how this compound can be used for covalent functionalization of SWCNTs.[9,17] The application of this reactant was found to facilitate the introduction of luminescent defects into SWCNTs,[9] and the reaction conditions strongly influenced the resulting properties of BPO-modified SWCNTs.[17] Regrettably, despite the apparent structural simplicity of benzoyl peroxide (BPO), the underlying radical-driven chemical reactions exhibit considerable complexity[18–22] and remain poorly understood, particularly in the context of nanomaterial functionalization. A thorough comprehension of these mechanisms is crucial, given the wide range of applications of BPO across diverse fields of chemistry.[23–25] While the application of BPO in the functionalization of SWCNTs provides a relevant model system for analyzing these aspects, it should be acknowledged that only a narrow selection of BPO derivatives is commercially available. Having the ability to tune the chemical structure of BPO would enable gaining a more thorough understanding of the intricate nature of radical-based transformations. Concomitantly, such modifications would provide much more control over the physicochemical properties of BPO, including solubility, decomposition rate, chemical stability, and reactivity of the derived radicals[26–28] to identify better what are the application opportunities of this widely used chemical compound.

In response to these challenges, this study systematically explored the reactivity of a broad spectrum of self-synthesized BPO derivatives in the radical covalent functionalization of SWCNTs. By investigating how variations in the chemical structure of BPO derivatives (attachment of functional groups, *e.g.*, alkyl, alkoxyl, carbonyl, halide, nitrile, or nitro in various positions) affect the radical generation and SWCNT functionalization, we deepened the understanding of the fundamental mechanisms governing these processes. Through careful control of reaction conditions, including temperature and radical type/concentration, we elucidated their roles in the course and the extent of decay of BPO derivatives. From the nanocarbon perspective, this knowledge opens up new prospects for fine-tuning the optical properties of SWCNT for making transformative applications such as sensors[29] or room-temperature single-photon emitters.[30] Furthermore, considering the vast potential of BPO-derived radicals for organic and polymer chemistry, the deduced relationships are highly valuable for designing more effective chemical transformations through radical chemistry. Last but not least, the results of this extensive synthetic initiative finally clarify why the electron-deficient reactants are most valuable for enriching the optical properties of SWCNTs.

2. Experimental

A complete list of reagents, synthesis, and characterization procedures for polymers and peroxides used in this paper is provided in the SI.

2.1. Preparation of (6,5)- and (7,5)-enriched SWCNTs for functionalization

The near-monochiral (6,5) or (7,5) SWCNT were collected according to the method presented earlier.[31] Briefly, in a typical suspension process, 6 mg of PFO-BPy (poly(9,9-dioctylfluorene-*alt*-6,6′-bipyridine)) or 9 mg of PFO (poly((9,9-dioctylfluorene)) synthesized in-house were dissolved in 5 mL of toluene. The solution was then transferred to a glass vial with 1.5 mg of preweighted SWCNTs. The mixture was homogenized in an ice-cooled bath sonicator to break the SWCNT bundles. Then, tip sonication was conducted while the mixture was cooled in an ice bath to keep a temperature of approximately 5 °C, which enabled the individualization of SWCNTs. After sonication, the thick suspension was transferred to a conical tube and centrifuged to remove the bundled SWCNTs and polymer aggregates. Then, 90% of the supernatant containing chirality-enriched

(6,5) or (7,5) SWCNT fraction was transferred to a fresh vial for chemical modification and characterization.

2.2. Thermal functionalization of SWCNTs

The standard reaction consumed 1 mL of (6,5) or (7,5) SWCNTs diluted to 0.8 or 0.6 cm^{-1}, respectively (E_{11} optical absorbance at the peak maximum). The molar concentrations of SWCNTs were calculated using molar absorptivity coefficients.[32] In parallel, the selected BPO derivative (aryl peroxide) was dissolved in toluene (1 mL) to achieve the necessary concentration ranging from 0.32 to 40 mg mL^{-1}. Then, the indicated components were combined in a glass vial and immersed in a stirred hot bath kept at 70 or 100 °C. After an hour (unless indicated otherwise), the samples were removed, cooled down to room temperature, and analyzed.

2.3. Characterization of functionalized SWCNTs

Optical absorption spectra were recorded with a Hitachi U-2910 spectrophotometer using a quartz cuvette (5 mm path length) with a pure toluene-containing cuvette placed in the reference channel. The data were normalized to the peak of the E_{11} transition whenever necessary for comparison of chirality distribution.

PL excitation–emission maps were collected with a ClaIR plate reader (Photonetc. Inc.) equipped with supercontinuum laser EVO HP EU-4 (NKT Photonics) and bandpass filter LLTF Contrast (NKT Photonics). The following settings were used for analysis (exposure time: 100 ms, excitation: 460–900 nm, emission: 947–1650 nm). For PL measurements, SWCNTs were diluted so that their concentration in the measured samples was low, *i.e.*, 0.27 μg mL^{-1} (optical density of 0.15 in case of non-functionalized (6,5) SWCNTs) to avoid the inner-filter effect.[33] The PL spectra were extracted from the PL excitation–emission maps for the 574 nm excitation wavelength in case of (6,5) SWCNTs and 653 nm in case of (7,5) SWCNTs, normalized to the E_{11} or E_{11}^{*} intensity for spectral shape comparison, and fitted with a set of Voigt functions using self-developed Python scripts (more details in SI). The area ratio of all defect-induced peaks to the E_{11} peak was used for the estimation of the relative defect density implanted in the SWCNTs.

To obtain Raman spectra of the modified SWCNTs, it was necessary to prepare highly concentrated dispersions before drop-casting. The solvent excess was removed by centrifugation as follows. At least 1 mL of a sample containing the SWCNT suspension (with E_{11} absorption in the range of 0.3–0.4 a.u. for pure SWCNTs) was mixed with 0.2 mL methanol (to promote precipitation of the SWCNTs) in a 2 mL conical tube and centrifuged. The supernatant generated from each sample was discarded after it was confirmed using PL excitation–emission mapping that it did not contain SWCNTs. The SWCNT material deposited in the conical tube was redispersed in 0.2 mL toluene by a 3-minute-long bath sonication and subsequently drop-casted on a glass substrate for characterization. The samples were characterized using a Renishaw inVia Raman microscope equipped with a 50× objective (Leica). The spectra were baseline-corrected and normalized to the maximum value of G peak intensity.

In addition, Fourier-transform infrared (FTIR) spectroscopy was employed to confirm the presence of newly introduced functional groups into SWCNTs. For this purpose, functionalized raw soot was filtered, dried, ground, blended with dry KBr (FTIR quality), and analyzed as KBr pellets. The recorded spectra provided direct evidence of covalent attachment of substituents, complementing the optical characterization. Full experimental details and spectra are given in SI (Sections S1.2.3 and Sections S2.7).

Finally, to provide a semi-quantitative assessment of the brightening effect upon functionalization, relative photoluminescence quantum yield (PLQY) measurements were performed using IR-1061 as a near-infrared reference dye. This approach enabled a reliable comparison of emission efficiencies between pristine and functionalized SWCNTs under identical conditions. The detailed methodology and complete datasets are reported in SI (Sections S1.2.4 and S2.11).

3. Results and discussion

While the commercial availability of BPO derivatives is somewhat limited, or the price thereof prohibitive in some instances, their synthesis at the laboratory scale presents a highly advantageous, reliable, and time-efficient alternative.[23] Adherence to specific safety protocols is paramount when handling peroxides to minimize the risk of premature decomposition. This risk can arise from contact with incompatible materials, such as acids, bases, metals, and certain polar organic solvents. It is recommended to limit reaction scales to 1–2 g. Furthermore, optimal storage conditions are essential, including the utilization of appropriately sized plastic containers and the avoidance of exposure to heat or radiation. The systematic application of these guidelines facilitates tonnage-scale production and utilization of BPO in industrial applications (as an active pharmaceutical ingredient, food additive, or radical initiator). At the same time, at the laboratory scale, it mitigates the risk of uncontrolled decay. The economic viability and ready availability of various carboxylic acids or their acid chlorides, commonly used as peroxide precursors, further enhance the attractiveness of this synthetic route (Fig. 1a).

The first step of the process is halogenation, which involves dissolving the carboxylic acid in a suitable solvent and stirring for just 1–4 hours at room temperature (or up to 40 °C) in the presence of a halogen donor such as thionyl chloride or oxalyl chloride. This is followed by the removal of volatile byproducts and excess reagents *via* simple evaporation. Then, the acyl chloride coupling process is performed with 30% H_2O_2 and NaOH solution, which is also not time-consuming (1–2 hours). Moreover, the advantage is that the high purity of the resulting products (90–99%) minimizes the need for complex purification procedures (*via* crystallization or column chromatography), simplifying the work-up to straightforward steps of

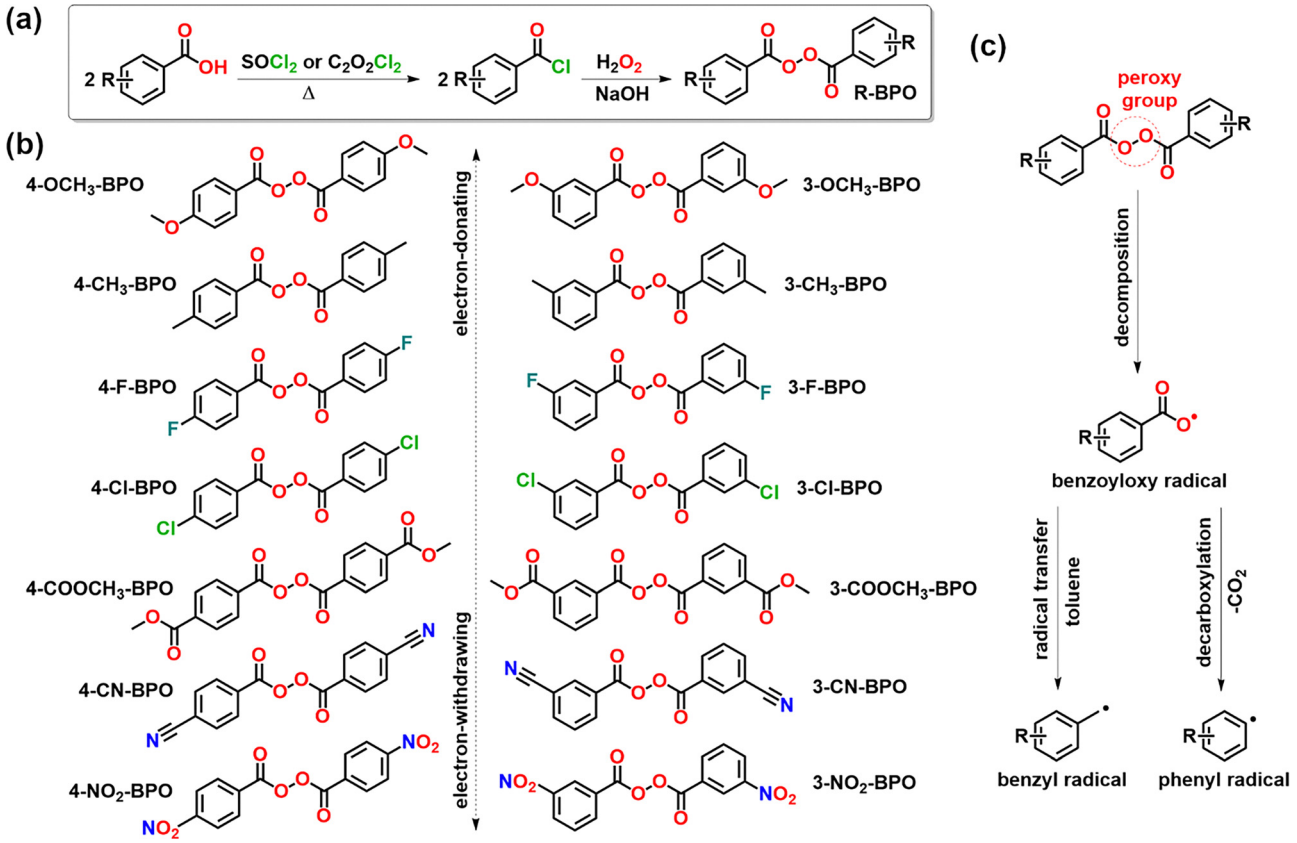

Fig. 1 (a) Synthetic approach used to obtain BPO derivatives, (b) a spectrum of BPO derivatives produced for SWCNT functionalization, (c) decomposition of BPO derivatives giving rise to the generation of radicals for SWCNT functionalization.

extraction, washing, and drying of the product. This approach enabled us to obtain a library of BPO derivatives (Fig. 1b and Table S1) within a short timeframe with high yields and low material costs, which possessed unique and tailored properties (for details, see Section S1.4 in the SI).

Then, the chirality-enriched (6,5) and (7,5) SWCNT dispersions were obtained in large amounts in toluene using our recently published multi-cycle CPE procedure with in-house synthesized PFO-BPy or PFO.[31] High structural order and chiral purity of the resulting materials were confirmed by Raman (Fig. S3a) and photoluminescence spectroscopy (Fig. S3b), making them suitable for studying how the addition of luminescent defects impacts the optical properties. Specifically, Raman spectroscopy showed low I_D/I_G band intensity ratios of *ca.* 0.02 for both SWCNT types, and PL excitation–emission analysis revealed a relatively small intensity of the photoluminescence sidebands (PSB)[34] both indicating minimal defect concentration and supporting the materials' high quality. The absorption spectra registered in the UV-vis-NIR range showed a predominance of the (6,5) and (7,5) chiralities, the E_{11} and E_{22} optical transition bands of which were recorded (Fig. S3c). Furthermore, UV-vis-NIR spectroscopy revealed only trace amounts of other chiral species as minor components. Consequently, the overall purity of the starting materials was estimated to be approximately 85–90%, making them well-suited for investigating the influence of intentionally introduced luminescent defects on the materials' optical properties. Having characterized the pristine SWCNT dispersions, we proceeded with the covalent functionalization of the SWCNTs using various self-synthesized BPO derivatives according to the provided procedure. The purified dispersions of SWCNTs wrapped by PFO-BPy6,6' polymer in toluene were reacted with BPO derivatives at 70 or 100 °C for 0.5–3 hours to create luminescent sp^3 defects. The molar ratios of the aryl peroxide to the SWCNTs ([R-BPO]/[CNT]) were in the range from 3 : 1 to 335 : 1 (details in Experimental section). Optimal initiator concentrations for different derivatives are provided in subsequent sections.

As we showed earlier, the primary species involved in this process are benzoyloxyl radicals, while benzyl and phenyl radicals (generated in side reaction with toluene/decarboxylation of benzoyloxyl radicals, respectively) contribute to a lesser extent (Fig. 1c).[17] The increase in density of benzoyloxy groups attached to the SWCNT surface generally translates to increased intensity of the defect peak located at *ca.* 1160 nm wavelength in the PL spectrum. Moreover, the above-mentioned secondary radicals, also capable of attacking the surface of SWCNTs and changing their optical properties, should be considered. In light of this spectral complexity, deconvolution of the defect E_{11}^* peak was performed for selected samples to estimate the

number and relative abundance of individual defect types (Fig. S4). For ease of reference in the present work, defects are generally referred to as E_{11}^{*} or, whenever possible, more precisely as $E_{11}^{*}(1160)$, $E_{11}^{*}(1220)$, *etc.*

To demonstrate the differences in reactivity between BPO derivatives for (6,5) SWCNT functionalization, we present results obtained under different peroxide concentrations after 1-hour reactions at 70 °C (Fig. S5) and 100 °C (Fig. S7) analogously to our former publication wherein only non-tailored BPO was used.[17] For better comparison of the spectral shapes of the obtained defect peaks, we also provide the same spectra normalized to E_{11}^{*} in Fig. S6 and S8, respectively. To systematically explore the behavior of various substituted BPOs, we analyze and compare them one by one in the following subsections (3.1–3.4), where different initiators are categorized according to their chemical structures and electronic character (as detailed in Section S2.5, and Table S3 in SI). The influence of this rather unrecognized factor on SWCNT functionalization efficiency and PL response is discussed thoroughly below, with key numerical data such as optimal reaction conditions, specific defect densities, and precise spectral shifts from Tables S2 and S4 in SI integrated into the discussion for clarity. The efficiency of SWCNT functionalization is further supported by evidence of radical-generating activity (Section S2.6 in SI) and direct attachment of chemical moieties (Section S2.7 in SI). Moreover, the kinetic control over the functionalization process, including defect stability, fluorescent properties, and the role of radical scavengers, is discussed in Section S2.8 in SI. Final characterization, encompassing the density of defects measured by Raman spectroscopy (Section S2.9 in SI), the dependence of PL redshift on Hammett substituent constant (Section S2.10 in SI), and validation of the brightening effect *via* relative PLQY measurements (Section S2.11 in SI) is also provided.

3.1. Carbon-based BPO substituents (4-CH_3, 3-CH_3)

The introduction of methyl substituents into the BPO structure provides an opportunity to assess how minor steric and electronic modifications affect the radical generation from variously modified BPOs and SWCNT functionalization efficiency. Due to its non-polar and weakly electron-donating (activating) nature, the methyl (–CH_3) group is expected to have minimal direct influence on radical stability but may affect decomposition pathways, *e.g.*, *via* chain transfer or the decarboxylation process (Fig. 1c), or alter steric accessibility of the reactive center in the case of the 3- substituent. At 70 °C, neither BPO nor its methyl derivatives facilitated high-density defect implantation, as evidenced by the low intensity of the E_{11}^{*} features in the PL spectra (Fig. 2a–c). It should be noted that the functionalization process with BPO or 3-CH_3-BPO required an extremely high molar excess, *i.e.*, ([R-BPO]/[CNT] = 168 : 1 or 84 : 1), to reach an evident increase in the intensity of the E_{11}^{*} peak. Importantly, no functionalization was observed for 4-CH_3-BPO (Fig. 2c) at this temperature, regardless of the concentration used. These findings suggested that at 70 °C, either the radical formation process or the reactivity of the formed radicals was insufficient to drive covalent functionalization of SWCNTs.

To explain this observation, we compared the Hammett constants (summarized in Table S3) for BPO (-H) and its 4-CH_3 and 3-CH_3 derivatives. The values for BPO and 3-CH_3-BPO are similar ($\sigma = 0$ and $\sigma = -0.069$, respectively), whereas the 4-CH_3-BPO displays a lower Hammet constant value of $\sigma = -0.170$ (Fig. 2d). Hence, the reactivity of the system was somehow related to the Hammet constants of the substituents. The 4-CH_3 ring-activating group hindered the possibility of SWCNT functionalization, confirming that the electron density distribution significantly influences radical reactivity and possibly its formation and decarboxylation rate.[35] This is reflected in the Atom-Centered Charges on the carbon atom adjacent to the carbonyl group (Table S3), indicated in red in Fig. 2e. For the 4-CH_3-BPO reactant, the partial positive charge is slightly lower (0.062) than in the other cases (0.068 for 3-CH_3-BPO and 0.067 for unsubstituted BPO). This difference in electron density at the *ortho* and *para* positions relative to the CH_3 group is attributed to the resonance effects.[36] The lowest reactivity of the electron-donating 4-CH_3 substituent, which is supposed to *activate* the molecule, deserves clarification. Hammet substituent constants, whether ring-activating or deactivating, are considered from the perspective of a possible electrophilic attack. However, radicals can be either electrophilic or nucleophilic, depending on their structure[37] which, as will be shown in this study, can significantly affect their capacity for SWCNT modification. Hence, the customarily defined activating nature of a given substituent does not necessarily mean that it will promote the functionalization of SWCNTs.

When the reaction of SWCNTs with the same compounds was conducted at 100 °C, distinct defect-related PL peaks emerged for all three reactants examined (Fig. 2f–h), indicating the successful incorporation of a broad range of sp^3-hybridized defects into the SWCNT lattice. The E_{11}^{*}/E_{11} area ratios (corresponding to the specific defect densities in SWCNTs[38]) were lower in the case of 4-CH_3-BPO processed at 100 °C than the corresponding values for BPO and 3-CH_3-BPO (Fig. 2i), confirming that the electron-donating properties of this substituent reduce electrophilicity of the resulting benzoyloxyl radical, making it less potent agent for SWCNT functionalization.[27,39] Up to the 84 : 1 molar ratio, the obtained PL spectra for both 3- and 4-CH_3-BPO closely resembled those obtained using non-substituted BPO. At a high radical excess of 168 : 1, SWCNT functionalization accelerated, judging by the elevated E_{11}^{*}/E_{11} ratios, and a new peak emerged at *ca.* 1130 nm, particularly for 4-CH_3-BPO (Fig. 2h). This feature is consistent with previously reported signatures of benzyl radicals attached to SWCNTs.[40] Since this effect was also observed for the 3-OCH_3 substituent (in addition to 4-CH_3 and unsubstituted BPO), this phenomenon will be discussed collectively in the next section. At this point, we would like to stress that these additional defect peaks only emerge at very high covalent modification temperatures (100 °C) and require substantial radical concentrations, which is not an issue in a typical approach.

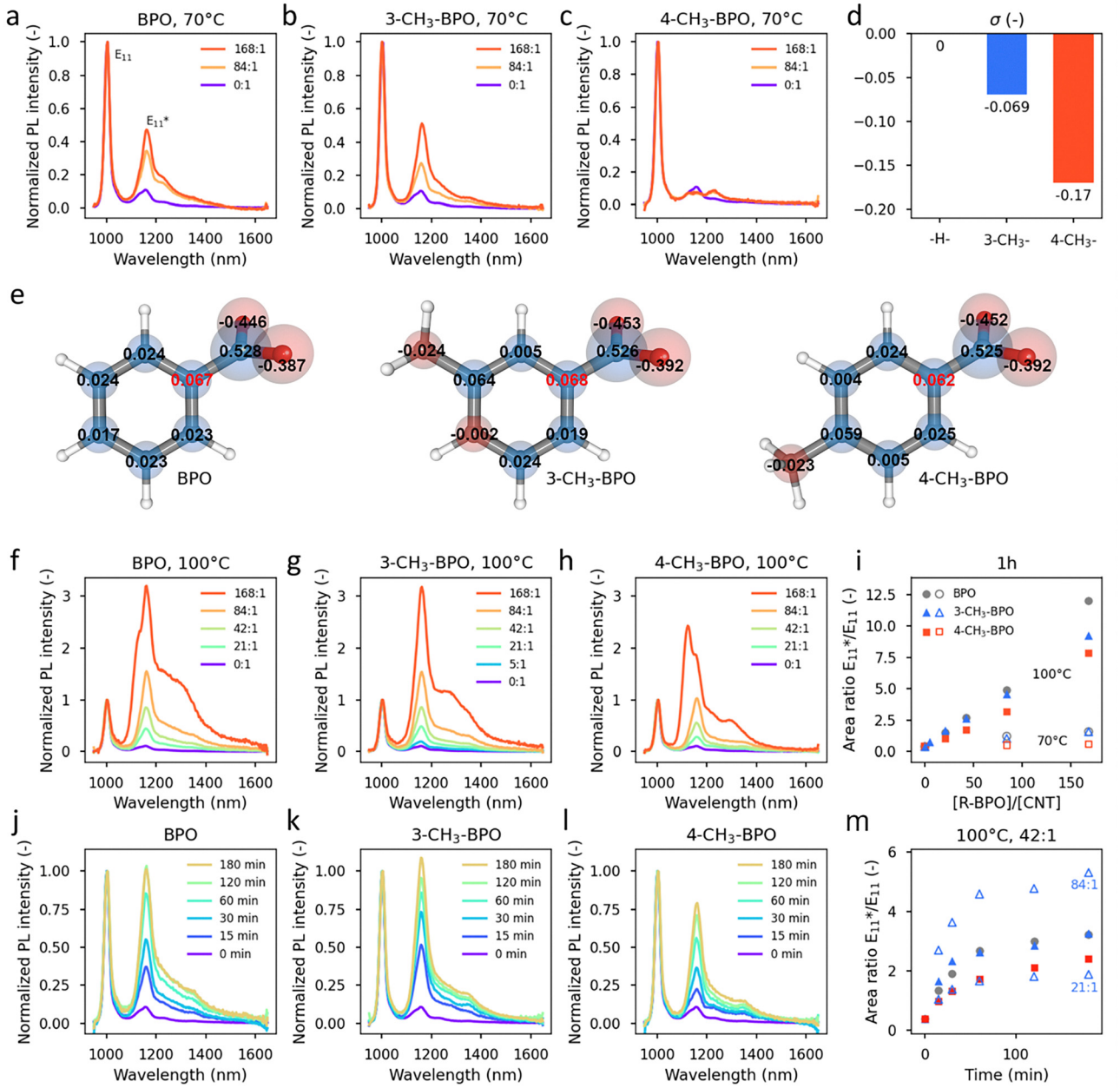

Fig. 2 PL spectra of SWCNTs functionalized using (a) unsubstituted, or (b) 3-CH_3- and (c) 4-CH_3- substituted BPO in 1 hour-long reaction at 70 °C, using different molar concentrations of radical initiators [R-BPO]/[CNT] (in legends). (d) Values of Hammet substituent constants. (e) Calculated Atom-Centered Charges for radicals derived from unsubstituted BPO, 3-CH_3-BPO, and 4-CH_3-BPO, f–h) PL spectra analogous to the ones presented in (a–c) but obtained at 100 °C. (i) The area ratios of E_{11}^*/E_{11} peaks in spectra from (a–c) and (f–h) *versus* [R-BPO]/[CNT] concentration ratios. For better visibility, values obtained using 3- and 4-substituted BPOs were plotted using triangles and squares, respectively. (j–l) PL spectra obtained for [R-BPO]/[CNT] = 42 : 1, after a given time in minutes. (m) Comparison of the increase in E_{11}^*/E_{11} area ratios with reaction time for [R-BPO]/[CNT] = 42 : 1 (full markers, the legend is the same as in i), but also 21 : 1 and 84 : 1 in case of 3-CH_3-BPO (empty markers).

A detailed analysis of the functionalization process under optimal conditions is shown in Fig. 2j–m. Selective SWCNT functionalization was performed using lower concentrations of radical source ([R-BPO]/[CNT] = 42 : 1) to monitor this process in greater detail. The E_{11}^*/E_{11} ratios stabilized after 3 hours of reaction for all three reactants, suggesting that, at this point, the radicals were almost wholly consumed. As expected, the 4-CH_3-BPO, weakly activated by the presence of the methyl group in the *para* position, produced the lowest SWCNT defect densities $\left(E_{11}^*/E_{11}\text{ area ratio} = 3.6\right)$. In contrast, the methyl group in the *meta* position did not seem to interfere with the reaction course $\left(E_{11}^*/E_{11} = 4.3\ vs.\ 4.6\text{ for unsubstituted BPO}\right)$, which will be explained in the subsequent parts of this article. At lower ratios of [R-BPO]/[CNT], adequately fewer defects were created, while at higher ratios, we again observed an accelerated reaction rate, manifested by a more rapid increase in the

E^*_{11}/E_{11} area ratios, and overall, a greater defect density (Fig. 2m).

3.2. Oxygen-containing BPO substituents (4-OCH_3, 3-OCH_3, 4-$COOCH_3$, 3-$COOCH_3$)

To understand the underlying relationships between the structure and reactivity of BPO derivatives more thoroughly, oxygen-containing substituents were engaged, which can affect the electronic characteristics of BPO derivatives to a greater extent.[28] The introduction of methoxy (-OCH_3) substituents into the BPO structure provided an opportunity to assess how stronger electron-donating functional groups influence radical formation and SWCNT functionalization. The Hammett constant indicated that 4-OCH_3 ($\sigma = -0.268$) was the most electron donating (ring-activating to electrophiles) substituent among those tested, whereas 3-OCH_3 ($\sigma = 0.115$) had a weakly electron withdrawing (ring-deactivating to electrophiles) nature. Despite this strong activating effect in electrophilic aromatic substitution reactions, the application of 4-OCH_3-BPO did not lead to the functionalization of SWCNTs under any tested conditions (Fig. S5 and S7). To confirm that this lack of functionalization was not due to an impaired radical generation process, additional experiments were performed using the chemical probe, 2,2-diphenyl-1-picrylhydrazyl (DPPH), as detailed in Section S2.6 in SI and Fig. S10. These results confirmed that radicals are indeed generated from 4-OCH3–BPO. This result stayed in accordance with earlier disclosed findings documenting that the weakly activated 4-CH_3-BPO compound was also not adequate for SWCNT modification. In contrast, placing the electron-rich methoxy group in the *meta* position (3-OCH_3-BPO) enabled significant functionalization at both high temperature (100 °C) and lower temperature (70 °C), provided that high radical concentrations were used. This effect can be explained by its weak electron-withdrawing characteristics with a much lower influence on the charge localized on a carbon atom adjacent to the carboxyl group (Fig. S9). Consequently, compared to the pristine BPO, the reactivity of 3-OCH_3-BPO was considerably higher. Very similar defect densities to BPO in molar excess over SWCNTs of 21 : 1 were obtained using 11 : 1 excess of 3-OCH_3-BPO (Fig. 3a). The optical spectra of the SWCNTs processed at both temperatures (70 °C and 100 °C) resembled that of the material treated with BPO (Fig. S5 and S7).

The spectrum of the material obtained at 100 °C for a substantial initiator excess over the SWCNTs (168 : 1) also included a contribution from a peak at *ca.* 1130 nm, as well as another secondary peak at 1300 nm. It should be noted that the latter was present in significantly higher amounts for 3-OCH_3-BPO and appeared at a lower molar excess of the

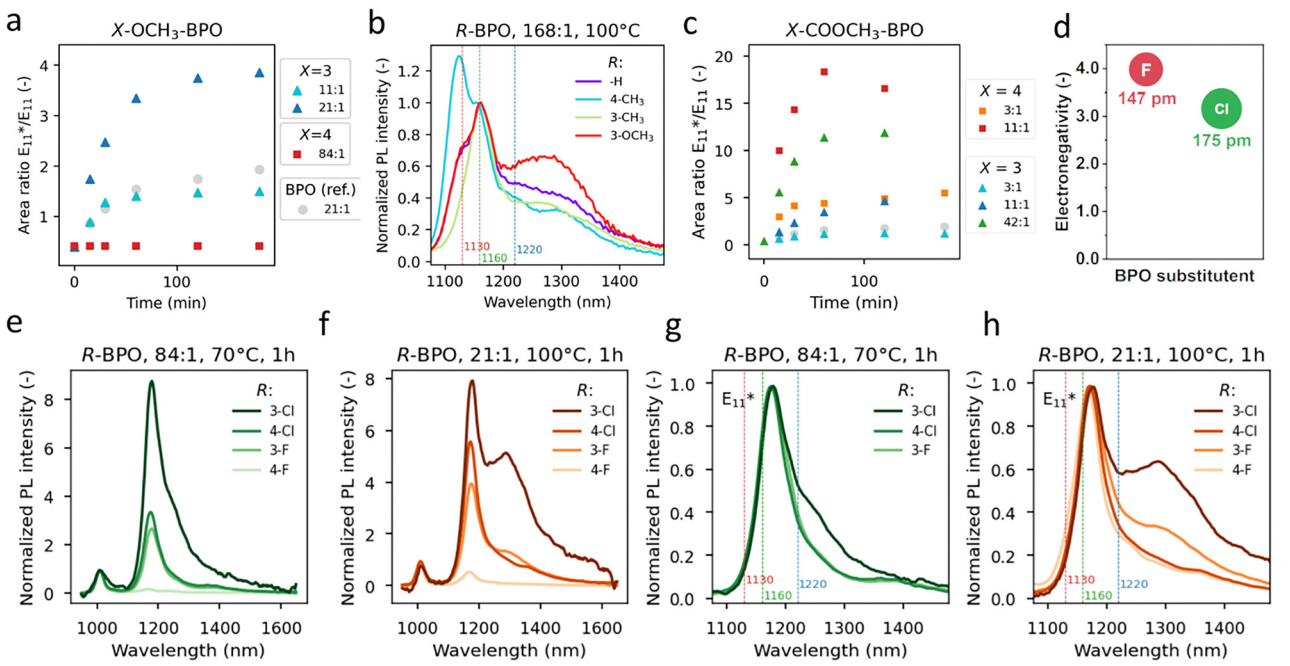

Fig. 3 Influence of oxygen-containing substituents on the course of SWCNT functionalization: (a) comparison of the increase in E^*_{11}/E_{11} area ratios with reaction time for 4- and 3-OCH_3-BPO compared to BPO. The reactions were conducted using different [R-BPO]/[CNT] concentration ratios listed in the legends. For better visibility, values obtained using 3- and 4-substituted BPOs were plotted using triangles and squares, respectively. (b) Comparison of spectral shapes of the defect region E^*_{11}, especially the $E^*_{11}(1130)$ peak, obtained with large excess of different initiators. (c) Comparison of the increase in E^*_{11}/E_{11} area ratios with reaction time for 4- and 3-$COOCH_3$-BPO as a function of BPO derivative concentration. Influence of halogen-derived substituents on the course of SWCNT functionalization: (d) comparison of electronegativity and van der Waals radii for F and Cl. Comparison of PL spectra obtained at (e) lower temperature but higher [R-BPO]/[CNT] and (f) higher temperature but lower [R-BPO]/[CNT] for -Cl and -F substituted BPO. (g) and (h) show spectral shapes of the E^*_{11} defect region in spectra from (e) and (f), respectively.

reactant to SWCNTs, proving higher reactivity of this BPO derivative. In our experiments, 4-CH_3-BPO exhibited the highest proportion of the peak at *ca.* 1130 nm, most likely corresponding to the benzyl modification of SWCNTs. This peak was also observed for unsubstituted BPO and 3-OCH_3-BPO, but under the investigated conditions, it did not appear for 3-CH_3-BPO (Fig. 3b). How can we explain the increased radical concentration of the benzyl radicals in the examined samples, which may give rise to this curiosity? BPO, which generates aryloxyl radicals, is prone to decarboxylation.[41,42] In turn, the rate of decarboxylation of aryloxyl radicals, yielding secondary phenyl radicals, increases along the series 4-F-Ph-$COO^{\bullet}$ $\leq$ 4-OCH_3-Ph-$COO^{\bullet}$ $<$ 4-CH_3-Ph-$COO^{\bullet}$ $\approx$ 4-Cl-Ph-$COO^{\bullet}$ $<$ $PhCOO^{\bullet}$ $<$ 3-Cl-Ph-$COO^{\bullet}$.[35] In light of the preceding, we speculate that the reduced electrophilicity of the 4-CH_3-Ph-$COO^{\bullet}$ radical, due to its electron-rich nature, is responsible for its prolonged lifetime because it is less likely to functionalize SWCNTs. At the same time, this provides a greater opportunity for a radical transfer reaction with the solvent (toluene). As a result, phenyl radicals can be converted into more stable benzyl radicals *via* the cage effect – the phenomenon where surrounding solvent molecules temporarily confine reactive intermediates, influencing their reaction pathways – leading to the more stable species.[22] The importance of benzoyloxyl radical electrophilicity also seems supported by the lack of reactivity observed for 4-OCH_3-BPO, even at a high reactant-to-SWCNT ratio of 84 : 1 (Fig. 3a). This compound is even more electron-rich due to the higher electron-donating capacity of the methoxy group positioned in the *para* position compared with the methyl moiety, which, as we presented above, did not favor SWCNT modification. Interestingly, prior research using diazonium salts successfully functionalized SWCNTs with the 4-OCH_3-Ph group,[43] a result not achieved herein for the corresponding BPO derivative. This observation reinforces the distinct reactivity difference between benzoyloxyl (obtained by BPO decay) and phenyl radicals (generated differently from diazonium salts) toward the SWCNT surface, mirroring their varied affinity for the polymerization of unsaturated monomers.[39] Nonetheless, it should be noted that, in contrast to substituents in the 4-position, a substituent in the 3-position, such as a methyl or methoxy group, cannot engage in direct resonance stabilization with the radical center on the carboxyl group. Hence, despite the electron-donating nature of the methoxy group, 3-OCH_3-BPO functionalizes SWCNTs with a reactivity similar to that of unsubstituted BPO, unlike its highly deactivated 4-OCH_3 counterpart.

With this point clarified, let us turn to the analysis of ester substituents, which offer an insightful extension to the study of substituent effects. They are interesting because they are functional groups with both inductive and resonance effects. When the ester group is connected *via* its carbonyl carbon (*i.e.*, forming a Ph–$COOCH_3$ moiety), the group exerts a strong electron-withdrawing influence due to a combination of a $-I$ (inductive) and a $-R$ (resonance) effects. This is reflected in its Hammett constants (σ = 0.37 and σ = 0.45, for 3- and 4-positioned substituents, respectively). 4-$COOCH_3$–BPO proved effective in introducing defects into the SWCNT lattice at both 70 °C and 100 °C, in contrast to either methyl ($\sigma = -0.17$ and $\sigma = -0.069$, for 4- and 3- substituents, respectively) or methoxy-substituted analog ($\sigma = -0.268$ and σ = 0.115, for 4- and 3-substituents, respectively) as well as unsubstituted BPO (σ = 0). For the treatment of SWCNTs with 4-$COOCH_3$–BPO at 100 °C, a defect density corresponding to an E_{11}^{*}/E_{11} area ratio of 3.4 was observed for one of the lowest radical concentrations ([R-BPO]/[CNT] = 3), indicating superior performance in covalent functionalization of SWCNTs. At the lower temperature of 70 °C, radical surface modification was still efficient, necessitating a much lower excess of radical initiator over SWCNTs (11 : 1) to reach a significant E_{11}^{*}/E_{11} area ratio of 4.3, compared to other BPO-based compounds. These results suggest that the electron-withdrawing character of the 4-$COOCH_3$ positively influences the reactivity of the 4-substituted benzoyloxyl radicals during SWCNT functionalization. In a related observation, the 3-substituted derivative, 3-$COOCH_3$–BPO, exhibited lower functionalization efficiency at 100 °C (E_{11}^{*}/E_{11} area ratio reaching 4.1 but for higher ratio [R-BPO]/[CNT] = 11) compared to its 4-isomer (Fig. 3c). Moreover, 3-$COOCH_3$ substituted BPO was much less effective also at 70 °C, even when a high molar excess of the initiator (84 : 1) was used. This behavior aligns with our previous findings, which indicated that both BPO derivatives modified in 3- and 4-positions lower the electron density of the aromatic ring. However, the 3-position is less electron-withdrawing because the resonance effect from the *meta* position cannot be effectively conjugated to the carbon atom bearing the peroxy group, unlike in the *para* isomer, and this difference results in the increased reactivity observed for 4-$COOCH_3$–BPO. The successful covalent attachment for 4-$COOCH_3$–BPO derivatives is further substantiated by FTIR analysis, which shows characteristic ester group vibrations after functionalization (Section S2.7 in SI).

Analysis of optical spectra from 100 °C (Fig. S7 and S8) highlights additional striking differences in both reactivity and characteristics of resulted optical spectra between methoxy- and ester-substituted peroxides, as well as the influence of functional group position. Whereas 3-$COOCH_3$-BPO displayed a well-resolved additional peak at 1300 nm, 4-$COOCH_3$–BPO did not show significant spectral features beyond the primary E_{11}^{*} defect registered at 1166 nm. Furthermore, the use of both 3-$COOCH_3$ and 3-OCH_3 for SWCNT functionalization led to a notable increase in the intensity of the peak at 1300 nm relative to optical spectra from unsubstituted BPO. We propose that this observation could be explained by the interaction of the substituent located in the 3-position with the SWCNT side wall. This interpretation stays in accordance with the findings of Yu *et al.*, who recently showed that similar proximal modification of SWCNTs induces strongly redshifted PL peaks.[44] This specific interaction, especially prevalent with highly reactive *meta*-substituted derivatives, can facilitate localized defect clustering and, at higher concentrations, lead to detrimental over-functionalization and fluorescence quenching, manifesting as increased noise and light scattering in the PL spectra (as thoroughly discussed in Section S2.8 in SI).

3.3. Halogen-containing BPO substituents (4-F, 3-F and 4-Cl, 3-Cl)

The introduction of halogen substituents into the BPO structure allows for a more in-depth evaluation of how electron-withdrawing groups with various atomic radii influence radical formation and (6,5) SWCNT functionalization efficiency. Fluorine and chlorine substituents are known to exert strong inductive effects while exhibiting limited resonance interactions. The Hammett constants indicate that 4-F (σ = 0.062) and 3-F (σ = 0.337) exert different electronic effects, with 3-fluorine being significantly more electron-withdrawing than its 4- counterpart. A similar trend is observed for chlorine, with 4-Cl (σ = 0.227) being less electron-withdrawing than 3-Cl (σ = 0.373).

At a lower temperature, both 3-Cl-BPO and 4-Cl-BPO, as well as 3-F-BPO, could introduce defects into the SWCNT lattice after 1 hour. When 4-F-BPO was used, no significant increase in E_{11}^{*} intensity was noticed, but prolonging the reaction time to 4 h revealed enhanced PL emission from the defect site. Even at 100 °C, this initiator requires the highest [R-BPO]/[CNT] ratios of up to 168 : 1, whereas, for the remaining derivatives, the optimal ratio is 21 : 1 or 5 : 1 (or slightly higher to achieve E_{11}^{*}/E_{11} area ratio 4–5). By comparing the spectra of SWCNTs functionalized in identical conditions at both 70 or 100 °C (Fig. 3e and f, respectively), the order of reactivity with halogen-substituted peroxides was as follows: 4-F-BPO ≪ 3-F-BPO < 4-Cl-BPO ≪ 3-Cl-BPO. Due to the significant excess of the radical initiator over SWCNTs in these reactions, we observed differences in spectral shapes of the E_{11}^{*} defect region, derived from both 4- and 3-substituted fluorine and chlorine derivatives (Fig. 3g and h), which can be attributed to their differing electronegativity and steric properties. The peak corresponding fluorescence at *ca.* 1130 nm was not observed in any case, whereas with increasing functional group size or for 3-position, the proportion of the band at *ca.* 1300 nm increased. Notably, for both 3-F and 3-Cl, this effect is apparent at much lower [R-BPO]/[CNT] molar ratios. At 100 °C, it is observed for 21 : 1 (Fig. 3h), in contrast to 4-Cl, where it is not observed until a reactant-to-SWCNT ratio of 84 : 1 is reached (Fig. S8). Fluorine, being the most electronegative element, exerts a more substantial inductive effect (Fig. 3d). However, its smaller atomic radius limits its electronic interactions with the SWCNT surface. Chlorine, while also electron-withdrawing, has a larger atomic radius, potentially altering steric interactions in the vicinity of the reaction site. These findings suggest that halogen substituents modulate radical reactivity through both electronic effects and steric hindrance. This underscores the importance of optimizing substituent placement, reaction mixture composition, and functionalization conditions when designing radical-based strategies for modifying SWCNT.

3.4. Nitrogen-containing BPO substituents (4-NO_2, 3-NO_2 and 4-CN, 3-CN)

Finally, the introduction of nitrogen-containing substituents, such as nitro (–NO_2) and cyano (–CN) groups, into the BPO structure provides insight into how strongly electron-withdrawing groups affect the radical formation process and SWCNT functionalization efficiency. Both substituents exhibit significant *-I* and *-R* effects, which influence the stability and reactivity of radical intermediates. The Hammett constants indicate that 4-NO_2 (σ = 0.778) and 4-CN (σ = 0.830) exert a strong electron-withdrawing influence, while their 3-counterparts, 3-NO_2 (σ = 0.720) and 3-CN (σ = 0.560), also significantly reduce electron density but to a lesser extent.

Functionalization experiments revealed that at 70 °C, all nitrogen-containing substituents were effective, although 4-NO_2-BPO required not only high initiator concentrations to achieve functionalization but also prolonged reaction time. The E_{11}^{*}/E_{11} area ratio correlated well with radical initiator concentration (Fig. S5). An exceptionally high peroxide concentration is required for 4-NO_2-BPO, exhibits low solubility in non-polar toluene. In contrast, significantly lower amounts are needed for 3-CN-BPO and 3-NO_2-BPO. Even at 3 : 1 [R-BPO]/[CNT] concentrations, these initiators are able to provide high defect densities. Interestingly, an enormous difference was noticed in the reactivity of NO_2-BPO, depending on the substituent position: higher defect densities were obtained with 3-NO_2-BPO at 70 °C (E_{11}^{*}/E_{11} area ratio of 3.5) for 3 : 1 molar excess of the initiator over the SWCNTs than for 4-NO_2-BPO at 100 °C for 168 : 1 ratio (E_{11}^{*}/E_{11} area ratio of 3.0, (Fig. 4a). Among tested initiators, the one substituted with the nitro group in the 3-position was the most reactive, while the one with the same group in the 4-position was one of the least reactive compounds examined. For SWCNTs subjected to a high concentration of 3-NO_2-BPO, uncontrolled functionalization occurs, manifesting as a jagged optical spectrum and, over time, complete fluorescence quenching (Fig. S5). This observation confirms published findings[45] that the process of SWCNT functionalization may be self-accelerating provided that reactant molecules are abundant, as the introduction of functional groups is more energetically favorable for covalently modified SWCNTs. As a result, multiple defects can accumulate in the affected region, ultimately compromising SWCNTs' optical properties. Therefore, it is crucially important to optimize the functionalization process so that the sources of radicals are completely consumed during SWCNT functionalization, or they need to be deactivated using radical scavengers, as discussed in detail in Section S2.8, SI.

At 100 °C, all nitrogen-containing initiators are active, displaying radical reactivities analogous to those observed at lower temperatures, *i.e.*, 4-NO_2-BPO ≪ 4-CN-BPO ≪ 3-CN-BPO < 3-NO_2-BPO (Fig. S7). Furthermore, the 3-substituted BPO derivatives require only small molar excesses, up to 11 : 1 and 3 : 1, respectively. This suggests that while both nitro and cyano groups withdraw electron density, positioning them at the 3-position, despite corresponding to lower Hammett constants, leads to more efficient covalent functionalization of SWCNTs. We hypothesize that this behavior stems from a combination of poor solubility of the 4-NO_2-BPO and 4-CN-BPO initiators in toluene, which limits their effective concentration and potentially the suboptimal reactivity profile of the derived radicals. While intense electron withdrawal of 4-isomers might be expected to increase reactivity, it could also lead to less selective radicals or faster decomposition pathways, whereas the

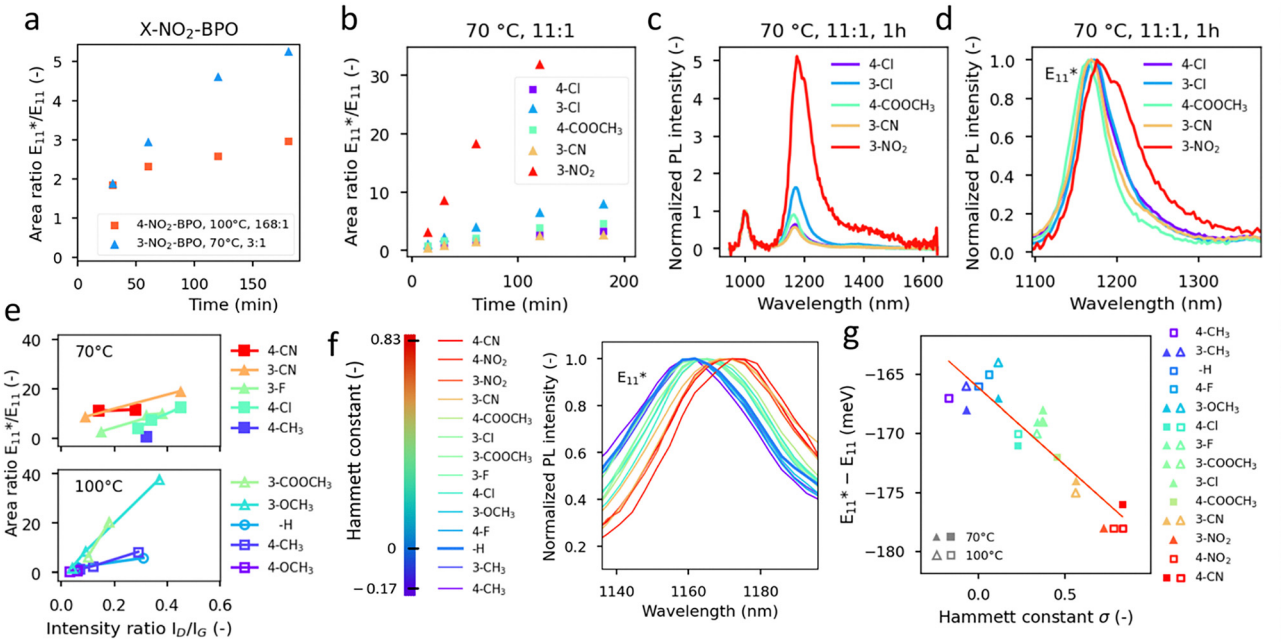

Fig. 4 (a) Increase in area ratio of defect E_{11}^* peak to original E_{11} obtained with 3-NO_2-BPO, compared to 4-NO_2-BPO. (b–d) Comparison of the reaction kinetics for the most reactive BPO initiators at the same temperature and with identical initiator-to-SWCNT molar ratios: (b) increase in area ratio of E_{11}^* peak to original E_{11} peak; (c and d) compared spectra obtained after 1 hour of reaction, normalized to E_{11} and E_{11}^* intensity, respectively. (e) Relationship between the E_{11}^*/E_{11} area ratio in PL spectra *vs.* intensity ratio of I_D/I_G peaks in Raman spectra for (6,5) SWCNTs (data in Table S4). Colors and order in legends correspond to the values of the Hammett substituent constant. Lines are plotted only to improve visibility. (f) Normalized E_{11}^* peaks of (6,5) SWCNTs obtained upon functionalization using benzoyloxyl radicals with different substituents. Line colors were selected in linear dependence on the Hammet substituent constant, as shown in the colorbar. (g) Close to the linear dependence of the experimentally observed optical trap depth on the Hammett constant. For better visibility, values obtained using 3- and 4-substituted BPOs were plotted using triangles and squares, respectively.

3-position offers a more effective balance between these processes. These findings highlight that although nitrogen-containing substituents are among the strongest electron-withdrawing groups tested, their influence on SWCNT functionalization strongly depends on their position within the BPO structure. The enhanced functionalization efficiency observed for 3-substituted derivatives suggests that fine-tuning electronic effects through substituent placement is crucial for optimizing defect formation in SWCNTs.

3.5. Direct comparison of most promising BPO derivatives and justification for their superior performance

We compared the functionalization kinetics, expressed as the E_{11}^*/E_{11} area ratio, for the most reactive initiators under identical conditions (70 °C and [R-BPO]/[CNT] = 11 : 1, Fig. 4b–d). It confirmed our previous observations that the most reactive initiators are those with 3-NO_2 and 3-Cl groups, even though they differ significantly in their Hammett constants. Both the Cl and NO_2 groups in the 3- position exhibit weak resonance effects on the electron density of the benzoyloxyl radical, while both exert electron-withdrawing influence *via* induction. In radical chemistry, aside from radical reactivity, stabilization often plays a crucial role in determining the outcome. Although NO_2 exhibits a more substantial electron-withdrawing effect, the stabilization of the radical in the 3-position is already sufficiently enhanced by a moderate *-I* effect (as in the case of Cl), allowing the radical to persist long enough to participate in SWCNT functionalization. The other substituents, *i.e.*, 4-$COOCH_3$ (σ = 0.450), 4-Cl (σ = 0.227), and 3-CN (σ = 0.560), exhibit significantly lower reactivity, with 4-$COOCH_3$ being slightly more reactive than the other two. The relatively higher reactivity of 4-$COOCH_3$ is most likely due to its strong resonance effect, which plays a less significant role in the reactivity of radical initiators in the 3- position. Regarding the values of full width at half-maximum (FWHM) of the E_{11}^* defect peaks, they remain consistent across all initiators after normalization (Fig. 4d), indicating a similar type of defect formation irrespective of the initiator structure. Importantly, the PL spectra of SWCNTs functionalized using BPO derivatives in many cases did not change even after months of storage, underscoring their robust nature. Such good stabilization was achieved by using a low initiator concentration and a high reaction temperature. A detailed description is provided in SI, Section S2.8.

To better understand the process of defect implementation, we also conducted Raman spectroscopy for selected modified (6,5) SWCNTs. The intensity ratios of D to G bands were calculated to assess the extent of SWCNT modification (Table S4). Then, the area ratios of E_{11}^*/E_{11} obtained for these samples were plotted against the I_D/I_G to compare the effectiveness of various substituted BPOs in imprinting the photoluminescent

defects. For SWCNTs functionalized at 70 °C, low E_{11}^*/E_{11} area ratios were noticed, but the I_D/I_G ratios indicative of the relative content of defects were high (Fig. 4e), suggesting an excessive amount of non-emissive defect states. Even 4-CH_3 substituted BPO, which did not exhibit the E_{11}^* defect feature, contained a considerable number of defects ($I_D/I_G \approx 0.32$ for [R-BPO]/[CNT] = 84 as well as 168). SWCNTs functionalized in a higher temperature range showed elevated values of E_{11}^*/E_{11} area ratio in relation to I_D/I_G ratios. Interestingly, SWCNTs functionalized at 100 °C with 4-OCH_3-BPO displayed both low E_{11}^*/E_{11} and I_D/I_G ratios even for overwhelming excess of the initiator [R-BPO]/[CNT] = 335, which indicates that either the radicals created in this reaction did not react effectively with the SWCNTs or the initiator remained largely intact. This latter possibility is improbable since the electron-donating effect of the methoxy group in 4-OCH_3-BPO is expected to cause significant dipole–dipole repulsion within the peroxy group, which dramatically decreases the thermal stability of the radical initiator.[28] Moreover, we discovered that with increasing the Hammett constant of the substituent, the same I_D/I_G corresponded to higher E_{11}^*/E_{11} ratios (Table S4). Based on this finding, we postulate that such reactants offer more effective implantation of the photoluminescent defects into SWCNTs.

Furthermore, while the influence of the substituent present in the moiety attached to the SWCNT on the optical properties of SWCNTs has been reported,[12,15,46] it is usually discussed only in the context of the optical trap depth it creates. At the same time, the possible impact of this factor on the propensity for SWCNT modification remains unknown. Considering that the electron-poor substituents better improve the PLQY of SWCNTs,[10] identifying the origins of this phenomenon is essential. To elucidate this, we subjected SWCNTs to chemical modification with 3-Cl-BPO, 3-F-BPO, and 4-F-BPO at 100 °C for 1 h and then analyzed the samples by Raman spectroscopy. Different positional isomers and two types of halogens were applied to tune the reactivity of the BPO derivatives. 4-F-BPO turned out to be the least reactive compound, giving an I_D/I_G ratio of 0.06 (Fig. 5a). As previously discussed, substituents in the 4- position are unable to deplete the electron density of the aromatic parts of BPO to a sufficient extent to promote the homolytic scission of this molecule, which is necessary to generate radicals for SWCNT modification. Consequently, the I_D/I_G ratio of 0.06 indicated a negligible degree of chemical modification of SWCNTs with 4-F-BPO, which was not much greater than that of pristine SWCNTs (0.02).

Hence, 3-isomers of halogenated BPO, the electronic configuration of which is more appropriate, were employed. As expected, 3-F-BPO functionalized performed better, and an I_D/I_G ratio of 0.18 was recorded. Furthermore, the chlorine-containing analog of this compound, *i.e.*, 3-Cl-BPO, made a much more substantial impact on the surface of SWCNTs, reaching an I_D/I_G ratio of 0.41. At the same time, the corresponding PL spectrum was of poor quality (Fig. 5b), confirming a considerable modification of the material. In light of the foregoing, the obtained results strongly suggest that treatment of SWCNTs with 3-Cl-BPO not only introduces deeper traps for mobile excitons (Fig. 5c and d), compared to the exposure to 4-F-BPO but also impacts the underlying photophysics. We hypothesize that the reported in the literature improvement of PLQY and E_{11}^*/E_{11} ratios related to the attachment of electron-withdrawing substituents to the SWCNT side wall[10] is likely caused by the increased amount of such groups on the SWCNT surface. The density of luminescent defects in SWCNTs is directly related to the I_D/I_G ratios measured by Raman spectroscopy[5,47] and the highest E_{11}^*/E_{11} ratios were recorded for the most severely affected SWCNTs, which were exposed to the electron-poor reactants containing substituents in the 3-position. Thus, in addition to the previously disclosed increased exciton trap depth for electron-deficient SWCNT addenda,[48] it should also be considered what happens when an exciton experiences thermal detrapping.[49] For these SWCNTs, which are supposedly more functionalized, it is likely that excitons, which generally have high mobility,[50,51] can become effectively retrapped by the defect sites present in abundance. Consequently, radiative recombination through the defect channel becomes much more probable, which

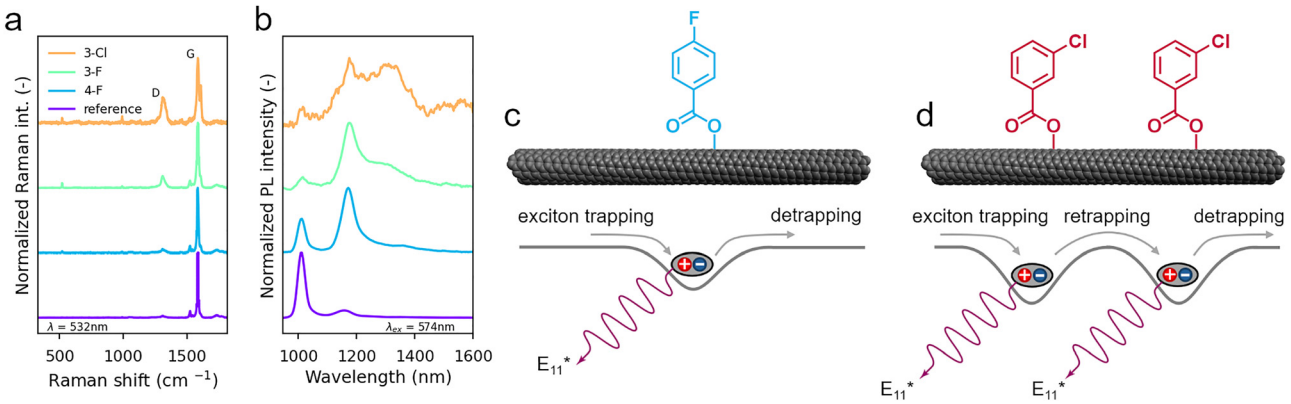

Fig. 5 (a) Raman spectra of pristine SWCNTs and modified with 3-Cl-BPO, 3-F-BPO, and 4-F-BPO, (b) corresponding PL spectra normalized to the intensity of the maximum of the peak of the highest intensity, SWCNT reacted with (c) 4-F-BPO, and (d) 3-Cl-BPO with the schematics of the main phenomena related to exciton dynamics in SWCNTs modified with luminescent defects.

explains why the E_{11}^* feature is much more pronounced in as-modified SWCNTs and why these very SWCNTs display leading PLQYs. The possibility of exciton retrapping is supported by a recent study by Sebastian *et al.*,[52] who reported that oxygen-based defects experience clustering on the SWCNT surface. It is likely that the benzoyloxy groups connected to SWCNTs also *via* oxygen may exhibit analogous clustering, thereby increasing the probability of the proposed exciton retrapping.

3.6. Relationship between the E_{11}^* peak position and the Hammett substitution constants

Upon closer examination of the E_{11}^* peak positions for various substituents, as exemplified in Fig. 4f, subtle variations in peak location are discernible depending on the substituent type and its position (3- *vs.* 4-). Considering that the functionalization approach involving the attachment of a functional group to SWCNTs *via* a carbonyl linker (SWCNT-O-C(O)-Ph-R) has not been previously investigated in this context, we aimed to address this gap and relate our findings to existing literature data for SWCNT-Ph-R type defects. For the analysis, we selected the spectra obtained with low concentrations of the initiator and exhibiting similar defect densities (Fig. S17). The E_{11}^*/E_{11} area ratios, as well as the positions of the peaks, were calculated using a model visualized in Fig. S4. Values obtained for all used peroxides were collected in Table S2. E_{11}^* peaks' intensities were normalized to show their exact positions and reveal that increasing the Hammett substituent constant indeed caused further redshift of the defect peak in PL spectra of modified SWCNTs (Fig. 4f). The relation between the Hammett substituent constant and the spectral shift (difference in spectral positions between E_{11}^* and E_{11} in nm, often referred to as the optical trap depth) is shown in Fig. 4g.

Our investigation into the effect of substituted benzoyloxy radicals on the photoluminescence of (6,5) SWCNTs reveals a complex interplay between substituent electronic properties, reaction temperature, and the resulting optical spectra modifications. In agreement with the general trend reported by Piao *et al.*[13] for aryl-functionalized SWCNTs dispersed by surfactants in water, we also observe progressing redshift of the E_{11}^* peak with increasing σ, linked with electron donating or withdrawing effect of substituents (Fig. 4f). This observation is consistent with the expected lowering of the LUMO energy level upon the introduction of electron-withdrawing functional groups. However, in contrast to the perfectly linear correlation reported by Piao *et al.*, our data demonstrate differences in this aspect, forming small groups with different Hammett constants but the similar E_{11}^* redshift, *e.g.* 4-CH_3, 3-CH_3, -H, 4-F and 3-OCH_3 (Fig. S18) or 4-Cl, 3-F, 3-$COOCH_3$ or 3-NO_2, 4-NO_2, 4-CN. This non-linearity is particularly evident at both low and high values of the Hammett substituent constants.

Furthermore, we observed noteworthy differences in the spectral shifts induced by 3- and 4-isomers (Table S2). For instance, the $E_{11}^* - E_{11}$ shift for 3-F and 4-F at 100 °C differs by 5 nm (160 nm *vs.* 155 nm) and for the ester group (160 nm *vs.* 165 nm). A minor $E_{11}^* - E_{11}$ shift difference (2 nm) was observed for SWCNTs modified with chlorine and cyano-substituted BPO, while methyl derivatives resulted in the same shift. This isomer-dependent behavior suggests that the position of the substituent on the benzoyloxyl radical subtly influences the local defect environment, which impacts the SWCNT electronic structure. These differences could arise from steric effects, variations in the spatial arrangement or orientation of the attached functional group relative to the SWCNT surface (potentially influenced by interactions within the conjugated polymer wrapping), or subtle changes in the electronic coupling between the substituent and the SWCNT lattice, depending on the *meta* or *para* orientation.

It is important to note that this observation is not entirely without precedent. Indeed, our previous studies on solvatochromism in polymer-dispersed SWCNTs have demonstrated the influence of solvents with varying dielectric properties. In those cases, solvent polarity, manifested as changes in the dielectric constant, was shown to interact with the polymer wrapping and induce additional strain effects. Consequently, the observed E_{11} peak shift was attributed to the combined influence of dielectric and strain interactions.[53] This indicates that the E_{11}^* defect peak shift observed in our study, induced by the attachment of moieties with differing dielectric properties, may also be mediated by alterations in the polymer wrapping of the SWCNT surface, thereby modulating its contribution to the observed spectral shift. However, polymer-free SWCNTs functionalized in water, as reported by Shiraki *et al.*,[15] also exhibit a different $E_{11}^* - E_{11}$ shift depending on the type of positional isomer used for their covalent modification, supporting that the observed effect is the result of the direct influence of the attached moiety on the SWCNT.

In summary, our findings demonstrate that while the electronic properties of benzoyloxyl radicals, as characterized by Hammett substituent constants, play a crucial role in tuning the E_{11}^* redshift, the relationship is not entirely linear and is significantly modulated by substituent position and to a lesser extent by the reaction temperature. This behavior highlights the complex interplay of factors governing SWCNT functionalization in polymer-organic solvent systems and underscores the potential for fine-tuning SWCNT optical properties by careful control of radical chemistry and reaction conditions.

3.7. Low-temperature (6,5) SWCNT functionalization with BPO derivatives

Given the sufficient radical activity at room temperature after thermal initiation, we aimed to examine if a further significant temperature decrease from 70 °C to 40 °C could extend the process duration and provide enhanced control. Functionalization at low temperatures presents a considerable challenge due to slower decomposition kinetics and potentially reduced radical reactivity. To assess the feasibility of such modifications, we investigated the functionalization of (6,5) SWCNT at 40 °C over an extended reaction period (24 h), using a high radical-to-SWCNT molar ratio of 251 : 1. The results, shown in Fig. 6a and b, provide insights into how different benzoyloxyl radicals

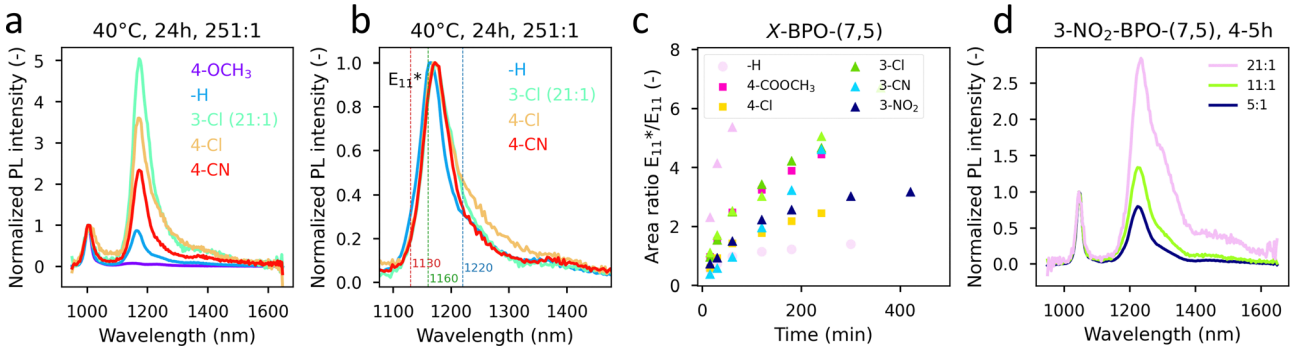

Fig. 6 PL spectra of (6,5) SWCNTs functionalized using BPO radicals substituted with groups listed in the legends, normalized to (a) E_{11} and (b) E_{11}^* PL intensity. Functionalization was conducted for a long time (24 h) at a low temperature (40 °C). A large molar ratio of initiator to SWCNTs (251 : 1) was necessary for the E_{11}^* to emerge in these conditions in case of all BPO derivatives except the most reactive 3-Cl-BPO (21 : 1). Spectra were obtained for 574 nm excitation wavelength. (c) E_{11}^*/E_{11} area ratios measured for (7,5) SWCNTs reacted with differently substituted BPO derivatives at 100 °C (except for 3-CN-BPO, which was reacted at 70 °C). For better visibility, values obtained using 3- and 4- substituted BPOs were plotted using triangles and squares, respectively. (d) Exemplary spectra of the (7,5) SWCNTs modified using different [R-BPO]/[CNT], obtained after 4–5 hours of reaction at 100 °C, normalized to E_{11} peak intensity. Spectra were obtained for 653 nm excitation wavelength.

and their derivatives influence defect formation under these conditions. Further details on the kinetic control over functionalization, defect stability, and the impact of radical scavengers are thoroughly discussed in Section S2.8 in the SI.

Among the tested initiators, the electron-rich 4-OCH_3-BPO remained inactive, failing to introduce detectable defects. In contrast, both chloro-substituted derivatives (3-Cl and 4-Cl) successfully generated E_{11}^* defects, albeit with distinct spectral features. Notably, 3-Cl-BPO produced broader defect-related peaks, resembling previous high-temperature experiments where excessive radical concentrations led to non-selective modifications, formation of defects with various morphologies, or defects accumulation in close vicinity to already installed moieties. A possible solution to this issue could be functionalization with a lower molar excess of these initiators while extending the reaction time to several days.

For 4-CN-BPO and unsubstituted BPO, the defect-induced peaks were among the narrowest recorded, indicating a more uniform functionalization pattern when the treatment was executed at a low temperature. However, this selectivity came at the expense of defect density, as indicated by the E_{11}^*/E_{11} area ratio, which reached *ca.* 2 for 4-CN-BPO and only *ca.* 1 for BPO. These findings suggest that while low-temperature functionalization enables the selective formation of defects, it necessitates prolonged reaction times and high radical concentrations, resulting in a trade-off between defect selectivity and density.

3.8. (7,5) SWCNT functionalization

The inherent differences in reactivity among BPO derivatives offer a powerful tool for achieving covalent functionalization of SWCNTs with various chiralities and, thus, reactivities. The significance of this capability may be used to enable the generation of E_{11}^* emission that is further redshifted towards the telecommunication band compared to functionalized (6,5) SWCNTs. While functionalization generally induces PL redshift and the emergence of new E_{11}^* peaks, the magnitude and nature of this spectral shift are dependent on the specific SWCNT chirality being modified.[12] Furthermore, SWCNT reactivity is known to substantially decrease with increasing SWCNT diameter because of reduced curvature and bandgap variation.[54,55]

As previously demonstrated, the functionalization process often does not terminate spontaneously upon initiation. Therefore, precise control over initiator reactivity, its tunability, and general performance becomes paramount. A crucial goal of achieving such control is to avoid detrimental over-functionalization, a condition known to quench the fluorescence of SWCNTs. Literature sources indicate that an optimal defect density range for enhanced photoluminescence is approximately 5–10 defects per 1000 nm.[48] Leveraging the tunable reactivity profiles of BPO derivatives presents a compelling strategy for achieving chirality-specific functionalization. For instance, the high reactivity of 3-NO_2-BPO can be effectively harnessed for the functionalization of (7,5) chirality, which is more challenging to modify due to increased diameter (d = 0.829 nm) and consequently lower reactivity compared to (6,5) SWCNTs (d = 0.757 nm). Fig. 6c and d provides a clear illustration of this principle. Additionally, other than 3-NO_2-BPO, less reactive BPO derivatives, such as 3-Cl-BPO and 4-Cl-BPO, provide a route to controlled functionalization of (7,5) SWCNTs, allowing for fine adjustments at low defect densities. Fig. 6c displays this approach, showcasing functionalization using BPO, 4-$COOCH_3$-BPO, 3-Cl-BPO, 4-Cl-BPO, 3-CN-BPO, and 3-NO_2-BPO at varied temperatures (70 °C and 100 °C) and concentrations (Fig. S20). Spectra obtained after 4–5 hours of reaction (Fig. 6d) highlight the concentration-dependent functionalization using 3-NO_2-BPO, with normalized spectra revealing a progressive increase in E_{11}^*/E_{11} peak area ratio and peak broadening at 1300–1320 nm. This controlled methodology, utilizing BPO derivatives with tailored reactivity, offers a

versatile toolkit for precise engineering the optical properties of even the less reactive SWCNTs for diverse applications.

4. Conclusions

Conducted investigations present a comprehensive view into the covalent functionalization of (6,5) SWCNTs (and in limited scope also (7,5) chirality) using a library of BPO derivatives with various substituents. Our findings highlight the unique control that can be achieved over the optical properties of SWCNTs through meticulous manipulation of radical chemistry and reaction parameters. A systematic exploration using a variety of self-synthesized BPO derivatives, including changes in the electron character of the substituent, steric hindrance, and positional isomerism (3- *vs.* 4-), elucidated the complex interaction between initiator structure and SWCNT functionalization efficiency.

In particular, the study showed that the electronic and steric properties of the substituted benzoyloxyl radical have a profound effect on SWCNT functionalization. The reactivity of various BPO derivatives was found to be highly dependent on the type of substituent, with electron-withdrawing groups generally increasing reactivity in both 3- and 4- positions. The 4-position of the substituent introduces more nuanced effects related to resonance stabilization. The carried-out investigations allowed for the identification of both highly reactive initiators, such as those containing 3-NO_2 or 3-Cl substituents, and less reactive counterparts, such as those containing 3-CH_3 or 4-F groups, enabling a tunable range of defect densities and spectral modifications. By exploiting the difference in reactivity of BPO derivatives, chirality-specific functionalization becomes a tangible goal, opening up the possibility of tailoring the optical properties of SWCNTs and potentially extending them toward the telecommunication window. Furthermore, the successful implementation of this methodology to the functionalization of (7,5) SWCNTs, which, due to its lower curvature, experiences lower reactivity, demonstrates the versatility of the developed synthetic toolbox. Interestingly, this study reveals that the SWCNTs modified with certain electron-poor substituents are more likely to experience exciton retrapping, which rationalizes why, in the literature, such-modified SWCNTs offer superior PLQY values and E_{11}^*/E_{11} ratios.

Additionally, our study highlights the key role of reaction conditions, especially temperature and initiator concentration, in achieving controlled functionalization. Kinetic studies have demonstrated that defect density can be precisely modulated, with lower initiator concentrations resulting in the complete depletion of radicals during the process and stable optical spectra for extended periods. Exploring functionalization at low temperatures (40 °C) further enhances the control regime, albeit at the expense of a trade-off between defect density and reaction time. Moreover, we explored strategies to terminate the functionalization process, including the use of radical scavengers. While TEMPO showed some promise in limiting further defect formation, precise control of initiator concentration proved to be a more reliable and cleaner approach to achieving stable functionalized SWCNT dispersion. The long-term stability of optical properties of such dispersions, even without post-reaction purification steps, further emphasizes the practical feasibility of this methodology.

The observed correlation between the E_{11}^* peak redshift and the Hammett substitution constants, although not strictly linear, provides a valuable framework for predicting and rationalizing the optical properties of functionalized SWCNTs. Differences in the value of the shift, compared to already published studies, highlight the system's complexity and provide insight into the interplay of electronic effects, such as steric hindrance, spatial arrangement at the defect site, and polymer wrapping.

In summary, our research provides the first comprehensive understanding of SWCNT functionalization based on modification of benzoyloxyl radical reactivity, offering a novel approach for the controlled engineering of luminescent defects. The presented systematic investigation, detailed kinetic studies, and exploration of substituent effects provide valuable insights into the surface chemistry of SWCNTs, paving the way for the rational design of nanomaterials for various optoelectronic applications. In parallel, the library of BPO derivatives synthesized in-house uncovered how, through modification of their structure, one can control the degree of their electrophilicity and, thus, the effectiveness of many fundamental chemical transformations in which BPO is regarded as an indispensable component.

Conflicts of interest

There are no conflicts of interest to declare.

Data availability

All data supporting this article have been included in the main text and SI. Supplementary information: Experimental details, characterization of the synthesized compounds and the isolated SWCNTs, additional PL spectra, properties of aryl peroxides, validation of radical-generating activity, FTIR spectroscopic evidence of covalent functionalization, estimation of the abundance of defects by Raman spectroscopy, approximation of PLQY, and functionalization of (7,5) SWCNTs. See DOI: **https://doi.org/10.1039/d5mh01129a**.

Acknowledgements

The authors would like to thank the National Science Centre, Poland (under the SONATA program, Grant agreement UMO-2020/39/D/ST5/00285) for supporting the research and Metropolis GZM, Poland (under Metropolitan Science Support Fund, Grant agreement No. RW/61/2025) for supporting the open access publication of the results of this study. The authors would also like to thank Marta and Alicja Kalyta for their help with preparing multiple functionalization reactions and Dominik Just for his help with Raman spectra measurements.

References

1 X. Wei, S. Li, W. Wang, X. Zhang, W. Zhou, S. Xie and H. Liu, Recent Advances in Structure Separation of Single-Wall Carbon Nanotubes and Their Application in Optics, Electronics, and Optoelectronics, *Adv. Sci.*, 2022, **9**(14), 2200054, DOI: 10.1002/advs.202200054.

2 T. Lei, I. Pochorovski and Z. Bao, Separation of Semiconducting Carbon Nanotubes for Flexible and Stretchable Electronics Using Polymer Removable Method, *Acc. Chem. Res.*, 2017, **50**(4), 1096–1104, DOI: 10.1021/acs.accounts.7b00062.

3 L. Wieland, H. Li, C. Rust, J. Chen and B. S. Flavel, Carbon Nanotubes for Photovoltaics: From Lab to Industry, *Adv. Energy Mater.*, 2021, **11**(3), 2002880, DOI: 10.1002/aenm.202002880.

4 A. Spreinat, M. M. Dohmen, J. Lüttgens, N. Herrmann, L. F. Klepzig, R. Nißler, S. Weber, F. A. Mann, J. Lauth and S. Kruss, Quantum Defects in Fluorescent Carbon Nanotubes for Sensing and Mechanistic Studies, *J. Phys. Chem. C*, 2021, **125**(33), 18341–18351, DOI: 10.1021/acs.jpcc.1c05432.

5 F. L. Sebastian, N. F. Zorn, S. Settele, S. Lindenthal, F. J. Berger, C. Bendel, H. Li, B. S. Flavel and J. Zaumseil, Absolute Quantification of Sp 3 Defects in Semiconducting Single-Wall Carbon Nanotubes by Raman Spectroscopy, *J. Phys. Chem. Lett.*, 2022, **13**(16), 3542–3548, DOI: 10.1021/acs.jpclett.2c00758.

6 P. Wang, J. Fortner, H. Luo, J. Kłos, X. Wu, H. Qu, F. Chen, Y. Li and Y. Wang, Quantum Defects: What Pairs with the Aryl Group When Bonding to the Sp^2 Carbon Lattice of Single-Wall Carbon Nanotubes?, *J. Am. Chem. Soc.*, 2022, **144**(29), 13234–13241, DOI: 10.1021/jacs.2c03846.

7 S. Settele, F. Stammer, F. L. Sebastian, S. Lindenthal, S. R. Wald, H. Li, B. S. Flavel and J. Zaumseil, Easy Access to Bright Oxygen Defects in Biocompatible Single-Walled Carbon Nanotubes via a Fenton-like Reaction, *ACS Nano*, 2024, **18**(31), 20667–20678, DOI: 10.1021/acsnano.4c06448.

8 D. Janas, Perfectly Imperfect: A Review of Chemical Tools for Exciton Engineering in Single-Walled Carbon Nanotubes, *Mater. Horiz.*, 2020, **7**(11), 2860–2881, DOI: 10.1039/D0MH00845A.

9 L. Przypis, M. Krzywiecki, Y. Niidome, H. Aoki and T. Shiraki, Enhancing near - Infrared Photoluminescence from Single - Walled Carbon Nanotubes by Defect - Engineering Using Benzoyl Peroxide, *Sci. Rep.*, 2020, 1–13, DOI: 10.1038/s41598-020-76716-9.

10 F. J. Berger, J. Lüttgens, T. Nowack, T. Kutsch, S. Lindenthal, L. Kistner, C. C. Müller, L. M. Bongartz, V. A. Lumsargis, Y. Zakharko and J. Zaumseil, Brightening of Long, Polymer-Wrapped Carbon Nanotubes by Sp 3 Functionalization in Organic Solvents, *ACS Nano*, 2019, **13**(8), 9259–9269, DOI: 10.1021/acsnano.9b03792.

11 F. J. Berger, J. A. de Sousa, S. Zhao, N. F. Zorn, A. A. El Yumin, A. Quintana García, S. Settele, A. Högele, N. Crivillers and J. Zaumseil, Interaction of Luminescent Defects in Carbon Nanotubes with Covalently Attached Stable Organic Radicals, *ACS Nano*, 2021, **15**(3), 5147–5157, DOI: 10.1021/acsnano.0c10341.

12 M. Kim, X. Wu, G. Ao, X. He, H. Kwon, N. F. Hartmann, M. Zheng, S. K. Doorn and Y. Wang, Mapping Structure-Property Relationships of Organic Color Centers, *Chem*, 2018, **4**(9), 2180–2191, DOI: 10.1016/j.chempr.2018.06.013.

13 Y. Piao, B. Meany, L. R. Powell, N. Valley, H. Kwon, G. C. Schatz and Y. Wang, Brightening of Carbon Nanotube Photoluminescence through the Incorporation of Sp3 Defects, *Nat. Chem.*, 2013, **5**(10), 840–845, DOI: 10.1038/nchem.1711.

14 B. J. Gifford, X. He, M. Kim, H. Kwon, A. Saha, A. E. Sifain, Y. Wang, H. Htoon, S. Kilina, S. K. Doorn and S. Tretiak, Optical Effects of Divalent Functionalization of Carbon Nanotubes, *Chem. Mater.*, 2019, **31**(17), 6950–6961, DOI: 10.1021/acs.chemmater.9b01438.

15 T. Shiraki, S. Uchimura, T. Shiraishi, H. Onitsuka and N. Nakashima, Near Infrared Photoluminescence Modulation by Defect Site Design Using Aryl Isomers in Locally Functionalized Single-Walled Carbon Nanotubes, *Chem. Commun.*, 2017, **53**(93), 12544–12547, DOI: 10.1039/C7CC06663E.

16 Y. Maeda, P. Zhao and M. Ehara, Recent Progress in Controlling the Photoluminescence Properties of Single-Walled Carbon Nanotubes by Oxidation and Alkylation, *Chem. Commun.*, 2023, **59**(98), 14497–14508, DOI: 10.1039/D3CC05065C.

17 P. Taborowska, A. Dzienia and D. Janas, Unraveling Aryl Peroxide Chemistry to Enrich Optical Properties of Single-Walled Carbon Nanotubes, *Chem. Sci.*, 2025, **16**(3), 1374–1389, DOI: 10.1039/D4SC04785K.

18 A. Zoller, D. Gigmes and Y. Guillaneuf, Simulation of Radical Polymerization of Methyl Methacrylate at Room Temperature Using a Tertiary Amine/BPO Initiating System, *Polym. Chem.*, 2015, **6**(31), 5719–5727, DOI: 10.1039/C5PY00229J.

19 C. G. Swain, W. H. Stockmayer and J. T. Clarke, Effect of Structure on the Rate of Spontaneous Thermal Decomposition of Substituted Benzoyl Peroxides, *J. Am. Chem. Soc.*, 1950, **72**(12), 5426–5434, DOI: 10.1021/ja01168a017.

20 M. Sankar, E. Nowicka, E. Carter, D. M. Murphy, D. W. Knight, D. Bethell and G. J. Hutchings, The Benzaldehyde Oxidation Paradox Explained by the Interception of Peroxy Radical by Benzyl Alcohol, *Nat. Commun.*, 2014, **5**(1), 3332, DOI: 10.1038/ncomms4332.

21 V. A. Yablokov, The Mechanisms of the Rearrangements of Peroxides, *Russ. Chem. Rev.*, 1980, **49**(9), 833–842, DOI: 10.1070/rc1980v049n09abeh002509.

22 Y. K. Syrkin and I. I. Moiseev, The mechanisms of some peroxide reactions, *Russ. Chem. Rev.*, 1960, **29**(4), 193–214, DOI: 10.1070/RC1960v029n04ABEH001227.

23 B. Her, A. Jones and J. W. Wollack, A Three-Step Synthesis of Benzoyl Peroxide, *J. Chem. Educ.*, 2014, **91**(9), 1491–1494, DOI: 10.1021/ed400240k.

24 Q. Hu, W. Li, C. Qin, L. Zeng and J.-T. Hou, Rapid and Visual Detection of Benzoyl Peroxide in Food by a Colorimetric and

Ratiometric Fluorescent Probe, *J. Agric. Food Chem.*, 2018, **66**(41), 10913–10920, DOI: 10.1021/acs.jafc.8b04733.

25 M. Sagransky, B. A. Yentzer and S. R. Feldman, Benzoyl Peroxide: A Review of Its Current Use in the Treatment of Acne Vulgaris, *Expert Opin. Pharmacother.*, 2009, **10**(15), 2555–2562, DOI: 10.1517/14656560903277228.

26 R. C. Lamb and J. R. Sanderson, Organic Peroxides. VIII. Kinetics and Free-Radical Efficiencies in the Thermal Decompositions of Some Mixed Isobutyryl-Substituted Benzoyl Peroxides, *J. Am. Chem. Soc.*, 1969, **91**(18), 5034–5038, DOI: 10.1021/ja01046a017.

27 M. E. Kurzu and M. Pellegrini, Electrophilic Properties of Benzoyloxy Radicals, *J. Org. Chem.*, 1970, **35**(4), 990–992, DOI: 10.1021/jo00829a027.

28 A. T. Blomquist and A. J. Buselli, The Decomposition of Sym-Substituted Benzoyl Peroxides, *J. Am. Chem. Soc.*, 1951, **73**(8), 3883–3888, DOI: 10.1021/ja01152a096.

29 S. S. Nalige, P. Galonska, P. Kelich, L. Sistemich, C. Herrmann, L. Vukovic, S. Kruss and M. Havenith, Fluorescence Changes in Carbon Nanotube Sensors Correlate with THz Absorption of Hydration, *Nat. Commun.*, 2024, **15**(1), 1–8, DOI: 10.1038/s41467-024-50968-9.

30 X. He, N. F. Hartmann, X. Ma, Y. Kim, R. Ihly, J. L. Blackburn, W. Gao, J. Kono, Y. Yomogida, A. Hirano, T. Tanaka, H. Kataura, H. Htoon and S. K. Doorn, Tunable Room-Temperature Single-Photon Emission at Telecom Wavelengths from Sp 3 Defects in Carbon Nanotubes, *Nat. Photonics*, 2017, **11**(9), 577–582, DOI: 10.1038/nphoton.2017.119.

31 P. Taborowska, A. Mielańczyk, A. Dzienia and D. Janas, Environmentally Conscious Highly Effective Sorting of Single-Walled Carbon Nanotubes Using Recurrent Conjugated Polymer Extraction, *ACS Sustainable Chem. Eng.*, 2025, **13**(1), 621–636, DOI: 10.1021/acssuschemeng.4c08836.

32 S. R. Sanchez, S. M. Bachilo, Y. Kadria-Vili, C. W. Lin and R. B. Weisman, N,m)-Specific Absorption Cross Sections of Single-Walled Carbon Nanotubes Measured by Variance Spectroscopy, *Nano Lett.*, 2016, **16**(11), 6903–6909, DOI: 10.1021/acs.nanolett.6b02819.

33 S. Kumar Panigrahi and A. Kumar Mishra, Inner Filter Effect in Fluorescence Spectroscopy: As a Problem and as a Solution, *J. Photochem. Photobiol., C*, 2019, **41**, 100318, DOI: 10.1016/j.jphotochemrev.2019.100318.

34 S. Settele, F. J. Berger, S. Lindenthal, S. Zhao, A. A. El Yumin, N. F. Zorn, A. Asyuda, M. Zharnikov, A. Högele and J. Zaumseil, Synthetic Control over the Binding Configuration of Luminescent Sp3-Defects in Single-Walled Carbon Nanotubes, *Nat. Commun.*, 2021, **12**(1), 2119, DOI: 10.1038/s41467-021-22307-9.

35 J. Chateauneuf, J. Lusztyk and K. U. Ingold, Spectroscopic and Kinetic Characteristics of Aroyloxyl Radicals. 2. Benzoyloxyl and Ring-Substituted Aroyloxyl Radicals, *J. Am. Chem. Soc.*, 1988, **110**(9), 2886–2893, DOI: 10.1021/ja00217a032.

36 J. Bromilow, R. T. C. Brownlee, D. J. Craik, M. Sadek and R. W. Taft, Nonadditive Carbon-13 Nuclear Magnetic Resonance Substituent Shifts in 1,4-Disubstituted Benzenes. Nonlinear Resonance and Shift-Charge Ratio Effects, *J. Org. Chem.*, 1980, **45**(12), 2429–2438, DOI: 10.1021/jo01300a033.

37 F. De Vleeschouwer, V. Van Speybroeck, M. Waroquier, P. Geerlings and F. De Proft, Electrophilicity and Nucleophilicity Index for Radicals, *Org. Lett.*, 2007, **9**(14), 2721–2724, DOI: 10.1021/ol071038k.

38 C. Ma, C. A. Schrage, J. Gretz, A. Akhtar, L. Sistemich, L. Schnitzler, H. Li, K. Tschulik, B. S. Flavel and S. Kruss, Stochastic Formation of Quantum Defects in Carbon Nanotubes, *ACS Nano*, 2023, **17**(16), 15989–15998, DOI: 10.1021/acsnano.3c04314.

39 J. C. Bevington and T. Ito, Reactivities of Monomers towards the Phenyl Radical, *Trans. Faraday Soc.*, 1968, **64**, 1329, DOI: 10.1039/tf9686401329.

40 Y. Maeda, S. Minami, Y. Takehana, J.-S. Dang, S. Aota, K. Matsuda, Y. Miyauchi, M. Yamada, M. Suzuki, R.-S. Zhao, X. Zhao and S. Nagase, Tuning of the Photoluminescence and Up-Conversion Photoluminescence Properties of Single-Walled Carbon Nanotubes by Chemical Functionalization, *Nanoscale*, 2016, **8**(38), 16916–16921, DOI: 10.1039/C6NR04214G.

41 M. Kling and S. Schmatz, Decarboxylation of Carbonyloxy Radicals: A Density Functional Study, *Phys. Chem. Chem. Phys.*, 2003, **5**(18), 3891–3896, DOI: 10.1039/b304544g.

42 B. Abel, J. Assmann, M. Buback, C. Grimm, M. Kling, S. Schmatz, J. Schroeder and T. Witte, Ultrafast Decarboxylation of Carbonyloxy Radicals: Influence of Molecular Structure, *J. Phys. Chem. A*, 2003, **107**(45), 9499–9510, DOI: 10.1021/jp0350823.

43 F. J. Berger, J. Lüttgens, T. Nowack, T. Kutsch, S. Lindenthal, L. Kistner, C. C. Müller, L. M. Bongartz, V. A. Lumsargis, Y. Zakharko and J. Zaumseil, Brightening of Long, Polymer-Wrapped Carbon Nanotubes by Sp^3 Functionalization in Organic Solvents, *ACS Nano*, 2019, **13**(8), 9259–9269, DOI: 10.1021/acsnano.9b03792.

44 B. Yu, S. Naka, H. Aoki, K. Kato, D. Yamashita, S. Fujii, Y. K. Kato, T. Fujigaya and T. Shiraki, Ortho -Substituted Aryldiazonium Design for the Defect Configuration-Controlled Photoluminescent Functionalization of Chiral Single-Walled Carbon Nanotubes, *ACS Nano*, 2022, **16**(12), 21452–21461, DOI: 10.1021/acsnano.2c09897.

45 B. M. Maciejewska, M. Jasiurkowska-Delaporte, A. I. Vasylenko, K. K. Kozioł and S. Jurga, Experimental and Theoretical Studies on the Mechanism for Chemical Oxidation of Multiwalled Carbon Nanotubes, *RSC Adv.*, 2014, **4**(55), 28826–28831, DOI: 10.1039/C4RA03881A.

46 T. Shiraishi, T. Shiraki and N. Nakashima, Substituent Effects on the Redox States of Locally Functionalized Single-Walled Carbon Nanotubes Revealed by in Situ Photoluminescence Spectroelectrochemistry, *Nanoscale*, 2017, **9**(43), 16900–16907, DOI: 10.1039/C7NR05480G.

47 F. L. Sebastian, F. Becker, Y. Yomogida, Y. Hosokawa, S. Settele, S. Lindenthal, K. Yanagi and J. Zaumseil, Unified Quantification of Quantum Defects in Small-Diameter Single-Walled Carbon Nanotubes by Raman Spectroscopy,

ACS Nano, 2023, **17**(21), 21771–21781, DOI: **10.1021/acsnano.3c07668**.

48 J. Zaumseil, Luminescent Defects in Single-Walled Carbon Nanotubes for Applications, *Adv. Opt. Mater.*, 2022, **10**(2), 2101576, DOI: **10.1002/adom.202101576**.

49 Y. Zheng, B. M. Weight, A. C. Jones, V. Chandrasekaran, B. J. Gifford, S. Tretiak, S. K. Doorn and H. Htoon, Photoluminescence Dynamics Defined by Exciton Trapping Potential of Coupled Defect States in DNA-Functionalized Carbon Nanotubes, *ACS Nano*, 2021, **15**(1), 923–933, DOI: **10.1021/acsnano.0c07544**.

50 A. J. Siitonen, D. A. Tsyboulski, S. M. Bachilo and R. B. Weisman, Dependence of Exciton Mobility on Structure in Single-Walled Carbon Nanotubes, *J. Phys. Chem. Lett.*, 2010, **1**(14), 2189–2192, DOI: **10.1021/jz100749c**.

51 L. Lüer, S. Hoseinkhani, D. Polli, J. Crochet, T. Hertel and G. Lanzani, Size and Mobility of Excitons in (6, 5) Carbon Nanotubes, *Nat. Phys.*, 2009, **5**(1), 54–58, DOI: **10.1038/nphys1149**.

52 F. L. Sebastian, S. Settele, H. Li, B. S. Flavel and J. Zaumseil, How to Recognize Clustering of Luminescent Defects in Single-Wall Carbon Nanotubes, *Nanoscale Horiz.*, 2024, **9**(12), 2286–2294, DOI: **10.1039/D4NH00383G**.

53 A. Dzienia, D. Just and D. Janas, Solvatochromism in SWCNTs Suspended by Conjugated Polymers in Organic Solvents, *Nanoscale*, 2023, **15**(21), 9510–9524, DOI: **10.1039/D3NR00392B**.

54 Y. Li, S. Osuna, M. Garcia-Borràs, X. Qi, S. Liu, K. N. Houk and Y. Lan, Reactivity of Single-Walled Carbon Nanotubes in the Diels–Alder Cycloaddition Reaction: Distortion–Interaction Analysis along the Reaction Pathway, *Chem. – Eur. J.*, 2016, **22**(36), 12819–12824, DOI: **10.1002/chem.201601799**.

55 Z. Chen, W. Thiel and A. Hirsch, Reactivity of the Convex and Concave Surfaces of Single-Walled Carbon Nanotubes (SWCNTs) towards Addition Reactions: Dependence on the Carbon-Atom Pyramidalization, *ChemPhysChem*, 2003, **4**(1), 93–97, DOI: **10.1002/cphc.200390015**.

